Journal of Sound and Vibration (2002) **253**(5), 1001–1014
doi:10.1006/jsvi.2001.4040 available online at http://www.idealibrary.com on IDEAL®

ANALYSIS OF A PIEZOELECTRIC MULTIMORPH IN EXTENSIONAL AND FLEXURAL MOTIONS

S. K. Ha and Y. H. Kim

Smart Structures and Materials Laboratory, Department of Mechanical Engineering, Hanyang University, 1271 *Sa1-Dong, Ansan, Kyounggi-do, Korea* 425-791.
E-mail: sungha@hanyang.ac.kr

(*Received* 29 *May* 2001, *and in final form* 24 *September* 2001)

Impedance and admittance matrices are presented for the analysis of the beam-type piezoelectric multimorph (PM). Each piezoelectric layer is polarized in the thickness direction. The stacking sequence can be arbitrary, and both the extensional and flexural motions are considered. The variational principle is used for deriving the lumped conjugate parameters: two mechanical ports for the extensional motion, four mechanical ports for the flexural motion, and m electrical ports for the m piezoelectric layers. The resonance and antiresonance frequencies are then easily calculated from the admittance matrices. For the case of all the piezoelectric layers either in series or parallel connection, the $m+6$ ports reduce to the seven ports, and its impedance and admittance matrices are presented. The present methods are applied to the cantilevered PM and their electromechanical behavior is studied. The tip trajectory of the cantilevered piezomotor is also investigated using the presented matrices. It is found that the present methods are very effective in analyzing the multilayer piezoelectric transducers.

1. INTRODUCTION

The piezoelectric unimorph and bimorph have been widely used in many applications, such as electroacoustic transducers, medical devices, microrobot, and atomic force microscope cantilevers due to the characteristics of miniaturization, high positioning accuracy, sensitive response, and large displacement [1–4]. However, they show, compared with piezoelectric stack actuator, disadvantages in generative force and response speed. Recently, to increase the converted mechanical energy per volume of piezoelectric material or to reduce the operating voltage, the piezoelectric multimorph (PM), i.e., the piezoelectric multilayer actuator in the extensional and flexural motions, has been designed and applied to air jet actuator [5] and piezomotor [6], etc.

The impedance and admittance matrices are often used in the analysis of piezoelectric transducers since the lumped parameters conveniently describe the electromechanical behavior and show the equivalent circuit of the transducers [7–10]. The resonance frequencies (RF) and the antiresonance frequencies (AF) which are very essential in the design of piezoelectric transducers [1, 11] can be effectively calculated using the admittance matrix.

Numerous investigations have been made into the analysis and design of the piezoelectric benders. Smits *et al.* [8, 9, 12] derived the dynamic admittance matrix and calculated the electrical and mechanical RF and AF together with the effective coupling factors of the cantilevered piezoelectric bimorph. Wang *et al.* [13–15] constructed the

0022-460X/02/$35.00

constitutive equations of symmetrical triple layer piezoelectric bimorph and discussed non-linear piezoelectric behavior and sensing effect of cantilevered unimorph and bimorph actuators. Rogacheva *et al.* [16] and Chang and Chou [17] investigated the electro-mechanical characteristics of symmetric and asymmetric piezoelectric bimorphs. Cho *et al.* [18] presented a five-port impedance matrix and equivalent electric circuit of piezoelectric bimorphs. Tanaka *et al.* [19] formulated basic equations for the multilayer piezoelectric beams in flexural motion using Hamilton's principle and Aoyagi *et al.* [20] presented a block equivalent circuit of bimorph with multiple elastic layer. However, impedance and admittance matrices of the PM are not reported until now.

In this paper, the differential equations for the extensional and flexural motions of the beam-type PM are decoupled and the mechanical and electrical boundary conditions are derived using the variational principle. A systematic procedure of deriving impedance and admittance matrices is then presented. Using the derived matrices, the characteristic equations are then presented, from which the resonance and antiresonance frequencies and eventually the effective electromechanical coupling factors (EECF) can be calculated. For the case of all the piezoelectric layers either in series or parallel, seven-port impedance and admittance matrices are also presented. In the numerical examples, the cantilevered PM in series or parallel connection is analyzed using the present methods and the tip trajectory of the cantilevered piezomotor is also investigated. The results are then compared with the three-dimensional finite element solutions. Excellent agreements are observed between the results by the impedance matrix and the finite element methods (FEM).

2. EQUATIONS OF MOTION AND BOUNDARY CONDITIONS

The cross-sectional view of the beam-type PM in the cartesian co-ordinate system x, y, and z is shown in Figure 1. The length, the width, the number of layers, and the thickness of the qth layer are denoted by ℓ, w, m, and $h^{(q)}$, respectively, and each layer can be either piezoelectric or non-piezoelectric. The PM is assumed to be so thin and narrow that the y and z direction dependent stresses vanish; the only non-zero stress is T_x. Each qth piezoelectric layer ($q=1,\ldots,m$) is polarized in the thickness direction, i.e., parallel to the z-axis, and metallized on the top and bottom faces of the piezoelectric layer, i.e., $z=z^{(q)}$ and $z=z^{(q-1)}$ so that the x and y directional electric fields also vanish. The one-dimensional constitutive equations for a piezoceramic is written as [21]

$$T_x = c_{11}S_x - e_{31}E_z, \qquad D_z = e_{31}S_x + \varepsilon_{33}E_z, \tag{1a, b}$$

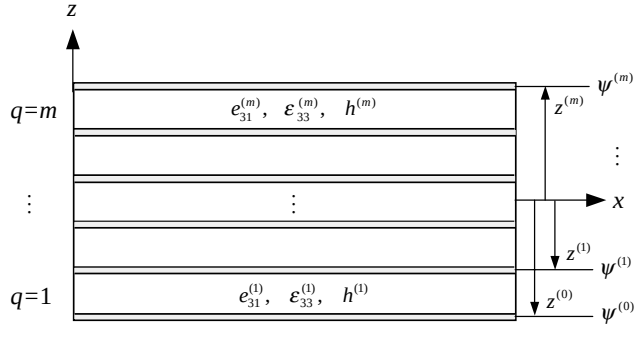

Figure 1. Configuration of the beam-type piezoelectric multimorph (PM). ▨, electrode; ▭, piezoelectric or non-piezoelectric layer.

where

$$c_{11} = \frac{1}{s_{11}^E}, \quad e_{31} = \frac{d_{31}}{s_{11}^E}, \quad \varepsilon_{33} = \varepsilon_{33}^T - \frac{d_{31}^2}{s_{11}^E}. \tag{2}$$

T_x and S_x in equation (1) are the axial normal stress and strain, and D_z and E_z are the electric displacement and field, respectively. c_{11} and $s_{11}^E$are the elastic stiffness and compliance under the constant electric field, e_{31} and d_{31} are the piezoelectric stress and strain constant, ε_{33} and ε_{33} are the dielectric constant under the constant strain and constant stress, respectively.

The extensional and flexural motions are considered, and the displacements, based on the Kirchhoff assumption, are assumed to be

$$u_x(x, z) = u_0(x) - zu_{z,x}, \qquad u_z(x, z) = u_z(x), \tag{3}$$

where the subscript x following a comma indicates the x directional spatial derivative. In equation (3), u_0 is the axial extensional displacement, i.e., the displacement u_x at the neutral axis ($z = 0$) that will be determined later. The strain–displacement relationship is then expressed as

$$S_x = u_{x,x} = u_{o,x} - zu_{z,xx}. \tag{4}$$

The electric field of the qth piezoelectric layer is approximated as

$$E_z^{(q)} = \frac{\psi^{(q)} - \psi^{(q-1)}}{h^{(q)}} = \frac{V^{(q)}}{h^{(q)}}, \tag{5}$$

where $\psi^{(q)}$ and $\psi^{(q-1)}$ are the electric potentials on the upper and lower electrodes of the qth layer, respectively.

The steady state responses of the PM are considered here. Therefore, the mechanical and electrical responses are assumed to be in harmonic motion with the same frequency as the excitation frequency ω and the time dependence term $e^{j\omega t}$ is omitted in the following derivation. The internal energy L for the motion of the PM is then defined as

$$L = \tfrac{1}{2}\int_{\upsilon} \{-\rho\omega^2(u_x^2 + u_z^2) + T_x S_x - D_z E_z\}\, \mathrm{d}\upsilon, \tag{6}$$

where υ denotes the total volume of the PM and ρ is the mass density. The variational principle yields

$$\delta L/w = \iint \{-\rho\omega^2(u_x\delta u_x + u_z\delta u_z) + T_x\delta S_x - D_z\delta E_z\}\, \mathrm{d}z\, \mathrm{d}x. \tag{7}$$

In the calculus of variations, u_0, u_z, and $V^{(q)}$ are considered as the independent variables. After substituting equation (3) into equation (7), the integration of the first term becomes

$$\iint \rho\omega^2(u_x\delta u_x + u_z\delta u_z)\, \mathrm{d}z\, \mathrm{d}x = \int_0^{\ell} \rho_h\omega^2(u_0\delta u_0 + u_z\delta u_z)\, \mathrm{d}x, \tag{8}$$

where the rotational inertia is neglected, and ρ_h indicates the mass density per unit length. The second term in equation (7), after integration by parts, becomes

$$\iint T_x\delta S_x\, \mathrm{d}z\, \mathrm{d}x = -\int_0^{\ell} N_{x,x}\delta u_0\, \mathrm{d}x + \int_0^{\ell} M_{x,xx}\delta u_z\, \mathrm{d}x + N_x\delta u_0\big|_0^{\ell} + M_x\delta u_{z,x}\big|_0^{\ell} + R_x\delta u_z\big|_0^{\ell}, \tag{9}$$

where the extensional load N_x, the flexural moment M_x, and the transverse shear force R_x are defined as

$$N_x(x) = \int T_x \, \mathrm{d}z, \quad M_x(x) = -\int T_x z \, \mathrm{d}z, \quad R_x(x) = -M_{x,x}. \tag{10a–c}$$

Using equation (5), the third term in equation (7) becomes

$$\iint D_z \delta E_z \, \mathrm{d}z \, \mathrm{d}x = \sum_{q=1}^{m} \int \int_{(q)} D_z^{(q)} \frac{\delta V^{(q)}}{h^{(q)}} \mathrm{d}z \, \mathrm{d}x = \sum_{q=1}^{m} Q^{(q)} \delta V^{(q)}, \tag{11}$$

where the charge of the qth layer is defined as

$$Q^{(q)} = \frac{1}{h^{(q)}} \int \int_{(q)} D_z^{(q)} \, \mathrm{d}z \, \mathrm{d}x. \tag{12}$$

Notice that the charge, as a conjugate parameter of voltage in equation (5), is represented by an averaged electric displacement through the thickness direction rather than by the value on the surface. Combining equations (8), (9), and (11) finally yields

$$\begin{aligned} \delta L/w = \int_0^{\ell} \{(-N_{x,x} - \rho_h \omega^2 u_0)\delta u_0 + (M_{x,xx} - \rho_h \omega^2 u_z)\delta u_z\} \, \mathrm{d}x \\ + N_x \delta u_0 \big|_0^{\ell} + M_x \delta u_{z,x} \big|_0^{\ell} + R_x \delta u_z \big|_0^{\ell} - \sum_{q=1}^{m} Q^{(q)} \delta V^{(q)}, \end{aligned} \tag{13}$$

which yield the extensional and flexural equilibrium equations:

$$N_{x,x} + \rho_h \omega^2 u_0 = 0, \qquad M_{x,xx} - \rho_h \omega^2 u_z = 0. \tag{14a, b}$$

As can be seen in equation (13), either force or displacement condition, each denoted in a vector form, $\mathbf{F}$ and $\mathbf{u}$, respectively, should be specified at the boundary:

$$\mathbf{F}_N = \begin{pmatrix} -N_x(0) \\ N_x(\ell) \end{pmatrix}, \qquad \mathbf{u}_N = \begin{pmatrix} u_0(0) \\ u_0(\ell) \end{pmatrix}, \tag{15a}$$

$$\mathbf{F}_F = \begin{pmatrix} -M_x(0) \\ -R_x(0) \\ M_x(\ell) \\ R_x(\ell) \end{pmatrix}, \qquad \mathbf{u}_F = \begin{pmatrix} u_{z,x}(0) \\ u_z(0) \\ u_{z,x}(\ell) \\ u_z(\ell) \end{pmatrix}. \tag{15b}$$

The last term in equation (13) also states that either electric charge or voltage should be given for each qth layer:

$$\mathbf{Q} = \begin{pmatrix} Q^{(1)} \\ \vdots \\ Q^{(m)} \end{pmatrix}, \quad \mathbf{V} = \begin{pmatrix} V^{(1)} \\ \vdots \\ V^{(m)} \end{pmatrix}. \tag{16}$$

Substituting equations (1b) and (4) into equation (12) yields the expression for the electric charge of each layer:

$$\begin{aligned} Q^{(q)} &= \frac{1}{h^{(q)}} \int \int_{(q)} e_{31}^{(q)} S_x \, \mathrm{d}z \, \mathrm{d}x + C^{(q)} V^{(q)} \\ &= e_{31}^{(q)} u_0 \big|_0^{\ell} - e_{31}^{(q)} z_c^{(q)} u_{z,x} \big|_0^{\ell} + C^{(q)} V^{(q)}, \end{aligned} \tag{17}$$

where $z_c^{(q)} = (z^{(q)} + z^{(q-1)})/2$ is the z directional co-ordinate of the center of the qth layer with respect to the neutral axis and $C^{(q)}$ is the clamped capacitance of the qth layer:

$$C^{(q)} = \ell \frac{\varepsilon_{33}^{(q)}}{h^{(q)}}. \tag{18}$$

Substituting equations (1a), (4), and (5) into equation (10) yields the following expressions for the extensional load and the flexural moment:

$$\begin{pmatrix} N_x \\ M_x \end{pmatrix} = \begin{bmatrix} A_{11} & B_{11} \\ B_{11} & D_{11} \end{bmatrix} \begin{pmatrix} u_{0,x} \\ u_{z,xx} \end{pmatrix} + \begin{pmatrix} N_x^* \\ M_x^* \end{pmatrix}. \tag{19}$$

The equivalent extensional load N_x^* and the equivalent flexural moment M_x^* due to the applied voltages are defined as

$$N_x^* = -\int e_{31} E_z \, \mathrm{d}z = -\sum_{q=1}^{m} e_{31}^{(q)} V^{(q)}, \qquad M_x^* = \int e_{31} E_z z \, \mathrm{d}z = \sum_{q=1}^{m} e_{31}^{(q)} z_c^{(q)} V^{(q)}. \tag{20a, b}$$

In equation (19), A_{11}, B_{11}, and D_{11} are defined as

$$A_{11} = \int c_{11} \, \mathrm{d}z = \sum_{q=1}^{m} c_{11}^{(q)} h^{(q)}, \qquad B_{11} = -\int c_{11} z \, \mathrm{d}z = -\sum_{q=1}^{m} c_{11}^{(q)} h^{(q)} z_c^{(q)}, \tag{21a, b}$$

$$D_{11} = \int c_{11} z^2 \, \mathrm{d}z = \sum_{q=1}^{m} c_{11}^{(q)} (h^{(q)} z_c^{(q)2} + h^{(q)3}/12). \tag{21c}$$

As can be seen in equations (14) and (19), the differential equations for the extensional and flexural motions can be decoupled by the vanishing B_{11}. This is made possible by properly choosing the position of $z = 0$, i.e., the neutral axis. Let z_0 be the distance from a reference axis, $\bar{z} = 0$, e.g. the bottom surface of the laminate, to the neutral axis, z=0. The distance z_0 is determined such that B_{11} vanishes:

$$B_{11} = -\sum_{q=1}^{m} c_{11}^{(q)} h^{(q)} (\bar{z}_c^{(q)} + z_0) = 0, \qquad z_0 = -\frac{1}{A_{11}} \sum_{q=1}^{m} c_{11}^{(q)} h^{(q)} \bar{z}_c^{(q)}. \tag{22}$$

Substituting equation (19) into equation (14) with the decoupled condition yields the decoupled extensional and flexural motion equations:

$$u_{0,xx} + \lambda_N^2 u_0 = 0, \qquad u_{z,xxxx} - \lambda_F^4 u_z = 0. \tag{23a, b}$$

The parameters λ_N and λ_F are the functions of the angular frequency ω and defined as

$$\lambda_N^2 = \frac{\rho_h \omega^2}{A_{11}}, \qquad \lambda_F^4 = \frac{\rho_h \omega^2}{D_{11}}. \tag{24}$$

3. IMPEDANCE AND ADMITTANCE MATRICES

In this section, the impedance and admittance matrices are derived using the results obtained in the previous section. Using equations (14)–(16), equation (13) can be now written as

$$\delta L/w = \begin{pmatrix} \mathbf{F}_N \\ \mathbf{F}_F \\ -\mathbf{Q} \end{pmatrix}^{\mathrm{T}} \delta \begin{pmatrix} \mathbf{u}_N \\ \mathbf{u}_F \\ \mathbf{V} \end{pmatrix}. \tag{25}$$

As can be seen in equations (23) and (24), only elastic stiffness is involved in the extensional and flexural motion equations for the PM. The general solution of equation (23) can be expressed as

$$u_0(x) = \mathbf{\Phi}_N \mathbf{A}_N, \qquad u_z(x) = \mathbf{\Phi}_M \mathbf{A}_F, \tag{26a, b}$$

where

$$\mathbf{\Phi}_N = (\cos \lambda_N x \quad \sin \lambda_N x), \tag{27a}$$

$$\mathbf{\Phi}_F = (\cos \lambda_F x \quad \sin \lambda_F x \quad \cosh \lambda_F x \quad \sinh \lambda_F x), \tag{27b}$$

$$\mathbf{A}_N = (A_1 \quad A_2)^{\mathrm{T}}, \qquad \mathbf{A}_F = (A_3 \quad A_4 \quad A_5 \quad A_6)^{\mathrm{T}}, \tag{27c, d}$$

where A_i are the coefficients to be determined using the boundary conditions.

As can be seen in equations (19) and (20), the extensional force can be represented as the functions of displacements and the voltages exerted on the piezoelectric element. Thus, the extensional forces at the ends $\mathbf{F}_N$ can also be given in terms of the functions of displacements at the boundary and the voltages. Using equations (19), (26a), (27a) and (27c), the extensional forces are expressed in a matrix form:

$$\mathbf{F}_N = \mathbf{B}_N \mathbf{A}_N + \mathbf{P}_N \mathbf{V}, \tag{28}$$

where the matrices $\mathbf{B}_N$ and $\mathbf{P}_N$ are defined as

$$\mathbf{B}_N = A_{11} \lambda_N \begin{bmatrix} 0 & -1 \\ -s_N & c_N \end{bmatrix}, \qquad \mathbf{P}_N = \begin{bmatrix} e_{31}^{(1)} & \cdots & e_{31}^{(m)} \\ -e_{31}^{(1)} & \cdots & -e_{31}^{(m)} \end{bmatrix}, \tag{29a, b}$$

where, for notation brevity, $c_N = \cos \lambda_N \ell$ and $s_N = \sin \lambda_N \ell$. The flexural forces at the ends $\mathbf{F}_F$ are also expressed in a matrix form similar to the extensional forces:

$$\mathbf{F}_F = \mathbf{B}_F \mathbf{A}_F + \mathbf{P}_F \mathbf{V}, \tag{30}$$

where the matrices $\mathbf{B}_F$ and $\mathbf{P}_F$ are defined as

$$\mathbf{B}_F = D_{11} \lambda_F^2 \begin{bmatrix} 1 & 0 & -1 & 0 \\ 0 & -\lambda_F & 0 & \lambda_F \\ -c_F & -s_F & m_F & n_F \\ -\lambda_F s_F & \lambda_F c_F & -\lambda_F n_F & -\lambda_F m_F \end{bmatrix}, \tag{31a}$$

$$\mathbf{P}_F = \begin{bmatrix} -e_{31}^{(1)} z_c^{(1)} & \cdots & -e_{31}^{(m)} z_c^{(m)} \\ 0 & \cdots & 0 \\ e_{31}^{(1)} z_c^{(1)} & \cdots & e_{31}^{(m)} z_c^{(m)} \\ 0 & \cdots & 0 \end{bmatrix}, \tag{31b}$$

where, for notation brevity, $c_F = \cos \lambda_F \ell$, $s_F = \sin \lambda_F \ell$, $m_F = \cosh \lambda_F \ell$, and $n_F = \sinh \lambda_F \ell$. The matrices in equations (28) and (30) are combined and expressed as follows:

$$\mathbf{F} = \mathbf{B}\mathbf{A} + \mathbf{P}\mathbf{V}, \tag{32}$$

where

$$\mathbf{F} = \begin{pmatrix} \mathbf{F}_N \\ \mathbf{F}_F \end{pmatrix}, \quad \mathbf{A} = \begin{pmatrix} \mathbf{A}_N \\ \mathbf{A}_F \end{pmatrix}, \quad \mathbf{B} = \begin{bmatrix} \mathbf{B}_N & 0 \\ 0 & \mathbf{B}_F \end{bmatrix}, \quad \mathbf{P} = \begin{bmatrix} \mathbf{P}_N \\ \mathbf{P}_F \end{bmatrix}. \tag{33}$$

Notice that the off-diagonal terms are zero in the matrix **B** since the extensional and flexural motions have been decoupled. Similar to the force and moment boundary conditions, the displacement boundary conditions of equation (15) can also be expressed in a vector form by using equations (26) and (27):

$$\mathbf{u} = \mathbf{G}\mathbf{A}, \tag{34}$$

where the displacement vector **u** and the matrix **G** are defined as

$$\mathbf{u} = \begin{pmatrix} \mathbf{u}_N \\ \mathbf{u}_F \end{pmatrix}, \quad \mathbf{G} = \begin{bmatrix} \mathbf{G}_N & 0 \\ 0 & \mathbf{G}_F \end{bmatrix}, \tag{35}$$

where

$$\mathbf{G}_N = \begin{bmatrix} 1 & 0 \\ c_N & s_N \end{bmatrix}, \quad \mathbf{G}_F = \begin{bmatrix} 0 & \lambda_F & 0 & \lambda_F \\ 1 & 0 & 1 & 0 \\ -\lambda_F s_F & \lambda_F c_F & \lambda_F n_F & \lambda_F m_F \\ c_F & s_F & m_F & n_F \end{bmatrix}. \tag{36}$$

As can be seen in equation (17), the electric charge of each qth piezoelectric layer has relationships with both the mechanical displacements and the electric voltages. Considering the definitions of $\mathbf{P}_N$ in equation (29b) and $\mathbf{P}_F$ in equation (31b), the charge vector in equation (25) can now be expressed as

$$\mathbf{Q} = -\mathbf{P}^{\mathrm{T}}\mathbf{u} + \mathbf{C}\mathbf{V}, \tag{37}$$

where the matrix **C** in equation (37) is a diagonal matrix with each qth diagonal term representing equation (18). Eliminating the coefficient vector **A** in equation (32) and using equation (37), we obtain

$$\begin{pmatrix} \mathbf{F} \\ \mathbf{Q} \end{pmatrix} = \begin{bmatrix} \mathbf{S} & \mathbf{P} \\ -\mathbf{P}^{\mathrm{T}} & \mathbf{C} \end{bmatrix} \begin{pmatrix} \mathbf{u} \\ \mathbf{V} \end{pmatrix}, \tag{38}$$

where

$$\mathbf{S} = \mathbf{B}\mathbf{G}^{-1}. \tag{39}$$

The forces and the displacements are the spatial and time-dependence variables. They are evaluated at the boundary and represented by the vectors. The velocities are also the spatial and time-dependence variables. For the derivation of the impedance matrix, the generic velocity vector **U** and current vector **I** are used instead of the generic displacement vector **u** and charge vector **Q**, respectively. Since we are considering all the physical quantities in a harmonic response, the following relations are used:

$$\mathbf{U} = \dot{\mathbf{u}} = \mathrm{j}\omega\mathbf{u}, \qquad \mathbf{I} = \dot{\mathbf{Q}} = \mathrm{j}\omega\mathbf{Q}. \tag{40}$$

where dots indicate differentiations with respect to time. It should be noticed that the time dependence $\mathrm{e}^{\mathrm{j}\omega t}$ has been omitted in the derivation. The velocity and charge vectors are the lumped conjugate parameters of the force and voltage vectors, respectively. The exchange of the charge vector for the voltage vector in equation (38) and using equation (40) easily yields the impedance matrix:

$$\begin{pmatrix} \mathbf{F} \\ \mathbf{V} \end{pmatrix} = \begin{bmatrix} \mathbf{Z}_M + \dfrac{1}{\mathrm{j}\omega}\mathbf{P}\mathbf{C}^{-1}\mathbf{P}^{\mathrm{T}} & \mathbf{Z}_C \\ \text{sym.} & \mathbf{Z}_E \end{bmatrix} \begin{pmatrix} \mathbf{U} \\ \mathbf{I} \end{pmatrix}, \tag{41}$$

where $\mathbf{Z}_M$ is the mechanical impedance matrix under the short circuit condition, $\mathbf{Z}_C$ is the electromechanical coupling impedance matrix, and $\mathbf{Z}_E$ is the electrical impedance matrix under the all clamped condition:

$$\mathbf{Z}_M = \frac{1}{\mathrm{j}\omega}\mathbf{S}, \qquad \mathbf{Z}_C = \frac{1}{\mathrm{j}\omega}\mathbf{P}\mathbf{C}^{-1}, \qquad \mathbf{Z}_E = \frac{1}{\mathrm{j}\omega}\mathbf{C}^{-1}. \tag{42a - c}$$

Exchanging the force vectors for the displacement vector in equation (38) and using equation (40) yield the admittance matrix:

$$\begin{pmatrix} \mathbf{U} \\ \mathbf{I} \end{pmatrix} = \mathrm{j}\omega \begin{bmatrix} \mathbf{S}^{-1} & -\mathbf{S}^{-1}\mathbf{P} \\ \text{sym.} & \mathbf{C} + \mathbf{P}^{\mathrm{T}}\mathbf{S}^{-1}\mathbf{P} \end{bmatrix} \begin{pmatrix} \mathbf{F} \\ \mathbf{V} \end{pmatrix}. \tag{43}$$

The admittance matrix in equation (43) enables us to calculate the mechanical and electrical responses of the transducers due to harmonic excitation by either forces at the boundary or voltages in each piezoelectric layer. It is observed in equation (43) that both the extensional and flexural motions can be generated by the exciting voltage because of the non-zero matrix $\mathbf{P}$. Equation (43) also facilitates the calculation of the mechanical and electrical RF and AF. In case of no external load, i.e., $\mathbf{F} = \mathbf{0}$, the lower right corner submatrix of equation (43) represents the multiport electrical admittance matrix $\mathbf{Y}(\omega)$ with components of Y_{ij} relating the ith current with the jth voltage:

$$\mathbf{Y}(\omega) = \mathrm{j}\omega(\mathbf{C} + \mathbf{P}^{\mathrm{T}}\mathbf{S}^{-1}\mathbf{P}). \tag{44}$$

The poles and zeros of $\mathbf{Y}(\omega)$ give the characteristic equations that yield the RF ω_r and the AF ω_a of electric current, respectively. The EECF k_{eff} is then calculated using the RF and the AF by applying the known expression [21]

$$k_{eff}^2 = \frac{\omega_a^2 - \omega_r^2}{\omega_a^2}. \tag{45}$$

In the cases of other boundary conditions than all mechanically free conditions considered above, the dimensions of the impedance matrix in equation (41) and the admittance matrix in equation (43) are reduced according to the specified displacement or force conditions [10]. The RF, the AF, and the EECF can then be calculated as above.

4. MULTIPLE CONNECTIONS

In the above derivation, the piezoelectric layers are assumed to be connected independently of each other. In general application, the electrical ports of the piezoelectric layers can be connected in either series or parallel. In this case, m electrical ports of the PM are reduced to one electrical port.

When all the electrical ports of the piezoelectric layers are connected in parallel, as shown in Figure 2(a), the voltages of the parallel connected layers have the same magnitude as externally applied voltage V_p and the currents of all the connected layers are summed to the current I_p entering the voltage supplier:

$$V^{(q)} = n^{(q)} V_p, \qquad I_p = \sum_{q=1}^{m} n^{(q)} I^{(q)}, \tag{46a, b}$$

where $n^{(q)}$ is 1 when the direction of applied voltage or current is the same as the direction of positive current or voltage; otherwise -1. By applying equation (46) to equation (38), the columns of the matrix $\mathbf{P}$ and the rows and columns of the matrix $\mathbf{C}$ in equation (38) are

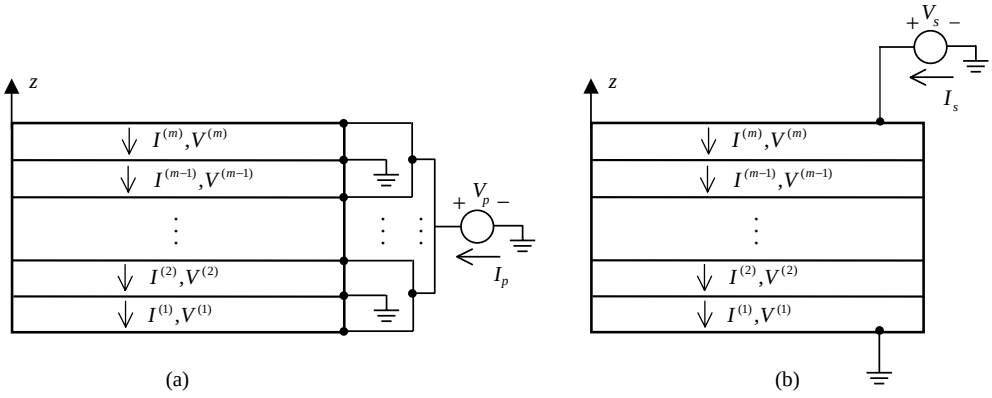

Figure 2. Multiple connections of the PM in parallel connection (a) and series connection (b).

now summed up:

$$\mathbf{P} = \left(\sum_{q=1}^{m} n^{(q)} e_{31}^{(q)} \quad -\sum_{q=1}^{m} n^{(q)} e_{31}^{(q)} \quad -\sum_{q=1}^{m} n^{(q)} e_{31}^{(q)} z_c^{(q)} \quad 0 \quad \sum_{q=1}^{m} n^{(q)} e_{31}^{(q)} z_c^{(q)} \quad 0 \right)^{\mathrm{T}}, \tag{47a}$$

$$\mathbf{C} = C_p, \tag{47b}$$

where C_p is the clamped capacitance of the PM in parallel connection;

$$C_p = \sum_{q=1}^{m} C^{(q)} = \ell \sum_{q=1}^{m} \frac{\varepsilon_{33}^{(q)}}{h^{(q)}}. \tag{48}$$

The impedance and admittance matrices of the PM in the parallel connection are still represented by equations (41) and (43), respectively, with **P** and **C** defined in equation (47).

For the series connection as shown in Figure 2(b), all the currents of the serially connected layers are the same as each other, denoted by I_s, and the voltages of the serially connected layers are summed to externally applied voltage V_s:

$$I_s = I^{(q)}, \qquad V_s = \sum_{q=1}^{m} V^{(q)}. \tag{49a, b}$$

The impedance matrix of the PM in series connection can be now obtained by applying equation (49) to equation (41): the columns of the matrix $\mathbf{Z}_C$ and the rows and columns of the matrix $\mathbf{Z}_E$ in equation (41) are summed up, i.e.,

$$\mathbf{Z}_C = \frac{1}{\mathrm{j}\omega} \left(\sum_{q=1}^{m} \frac{e_{31}^{(q)}}{C^{(q)}} \quad -\sum_{q=1}^{m} \frac{e_{31}^{(q)}}{C^{(q)}} \quad -\sum_{q=1}^{m} \frac{e_{31}^{(q)} z_c^{(q)}}{C^{(q)}} \quad 0 \quad \sum_{q=1}^{m} \frac{e_{31}^{(q)} z_c^{(q)}}{C^{(q)}} \quad 0 \right)^{\mathrm{T}}, \tag{50a}$$

$$\mathbf{Z}_E = \frac{1}{\mathrm{j}\omega C_s}. \tag{50b}$$

where C_s is the clamped capacitance of the PM in series connection;

$$C_s = \left(\sum_{q=1}^{m} \frac{1}{C^{(q)}} \right)^{-1} = \ell \left(\sum_{q=1}^{m} \frac{h^{(q)}}{\varepsilon_{33}^{(q)}} \right)^{-1}. \tag{51}$$

The admittance matrix of the PM in series connection can be now obtained by inversing the impedance matrix in equation (41) with $\mathbf{Z}_C$ and $\mathbf{Z}_E$ defined in equation (50). If some layers are connected in series and others in parallel, the derived equations can be accordingly applied to each layered group.

5. NUMERCIAL RESULTS

In this section, the impedance and admittance matrices derived in the previous sections are applied to three examples. G1195N piezoceramics and stainless steel are used for the piezoelectric layers and the shim layer, respectively. The material properties are as follows: for the G1195N, $1/s_{11}^E = 61{\cdot}0\,\text{GPa}$, $\rho = 7600{\cdot}0\,\text{kg/m}^3$, $v = 0{\cdot}3$, $d_{31} = 254{\cdot}0\,\text{pm/V}$, and $\varepsilon_{33}^T = 15{\cdot}0\,\text{nF/m}$; for the stainless steel, $1/s_{11}^E = 200{\cdot}0\,\text{GPa}$, $\rho = 7830{\cdot}0\,\text{kg/m}^3$, and $v = 0{\cdot}3$.

As a first example, the cantilevered PM with the shim layer, as shown in Figure 3(a), is considered. The length, the number of piezoelectric layers, and the total thickness of the PM are set to 75·0 mm, 10, and 5·0 mm, respectively. All the piezoelectric layers have the same thickness and they are connected in series. The effects of the thickness of the shim layer h_s on the electromechanical behavior of the PM are investigated. Under the statically exciting voltage, tip deflections and the blocking forces generated at the free end of the cantilevered PM are calculated for the various thickness ratios h_s/h_t, and the results are shown in Figure 3(b). As the thickness of the middle shim increases, the generative force by the exciting voltage increases monotonically and the bending rigidity of the bimorph increases exponentially, which results in the peak value of tip deflection when thickness ratio is 0·4. The variations of the RF, the AF, and the EECF for the various thickness ratios are shown in Figure 4(a) and 4(b). To verify the results by the present methods, three-dimensional FEM [22] are used. The element has four degrees of freedom at a node, i.e., three displacements and one electric potential. One hundred elements are used for the axial direction, and 20 elements for the thickness direction. In the finite element analysis, the tip deflection and the blocking force are calculated by the static analysis; the RF and the AF are calculated by the modal analysis under the condition of short circuit and open circuit, respectively [23]. Excellent agreements are shown in the results by the impedance matrix and the FEM.

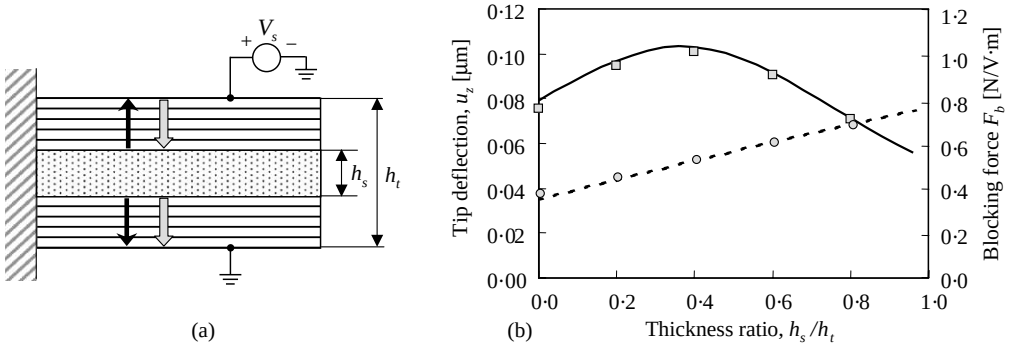

Figure 3. (a) The cantilevered PM in series connection with the shim layer ▨, shim layer; ▭ piezoelectric layer; ↑, poling direction, ⇧, electric field. The tip deflection u_z and blocking force F_b for the various ratios of the thickness of the shim layer to the total thickness h_s/h_t. ——, u_z (present); - - - -, F_b (present); ■, u_z (FEM); ●, F_b (FEM).

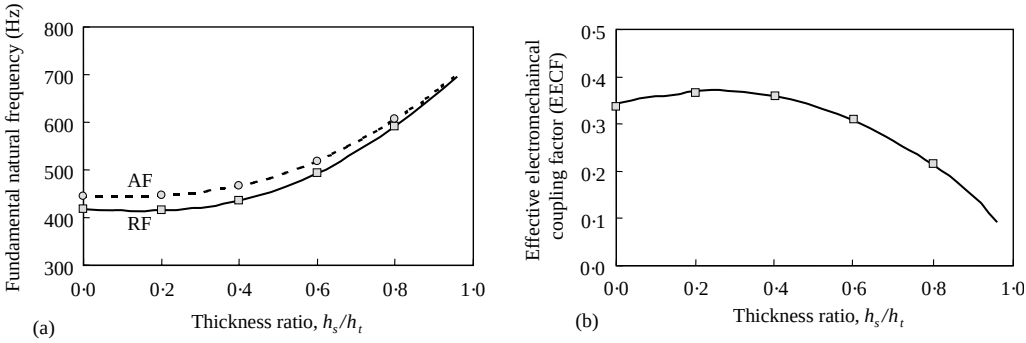

Figure 4. The resonance and antiresonance frequencies (a) and the effective electromechanical coupling factors (b) of the cantilevered PM in series connection for the various ratios of the thickness of the shim layer to the total thickness h_s/h_t; lines and symbols represent the results by the impedance matrix and the FEM respectively.

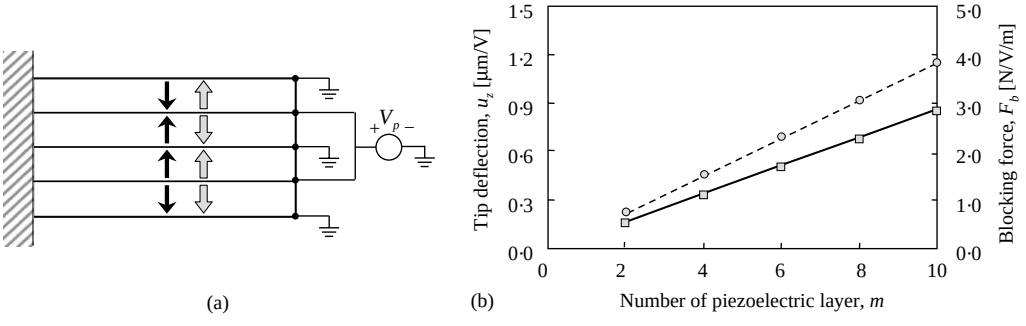

Figure 5. (a) The cantilevered PM in parallel connection for flexural motion only ($m=4$) ↑, poling direction; ⇧, electric field. The tip deflection u_z and blocking force F_b versus the number of piezoelectric layers: ——, u_z (present); - - - -, F_b (present); ■, u_z (FEM); ●, F_b (FEM).

In the second example, the cantilevered PM in parallel connection is considered. The length and the total thickness are set to 75·0 and 5·0 mm, respectively. All the layers are G1195N piezoceramics and connected in parallel. The poling direction of each piezoelectric layer is arranged in such a way that only flexural motion will be generated by the applied voltage, as shown in Figure 5(a). Under the statically exciting voltage, tip deflections and the blocking forces generated at the free end of the cantilevered PM are calculated versus the number of piezoelectric layers, and the results are shown in Figure 5(b). As the number of layers increases, both the displacement and blocking force increase monotonically. The variations of the RF, the AF, and the EECF versus the number of piezoelectric layers are shown in Figure 6(a) and 6(b). The results by the present method agree well with the finite element solutions.

In the final example, a multilayer piezomotor, as shown in Figure 7(a), is analyzed. The length, the thickness of the piezoelectric layer, and the number of piezoelectric layers are 10·0 mm, 0·1 mm and 10, respectively. All the layers are G1195N piezoceramics and they are electrically connected in such a way that the top and bottom piezoelectric layers are used to generate flexural motion by the applied voltage V_F and others are used to generate extensional motion by the applied voltage V_N. The applied voltages are $V_N = \cos \omega t$ V and $V_F = 2\cos(\omega t + \theta)$ V. The driving frequency ω is 2288·0 Hz which is half of the fundamental

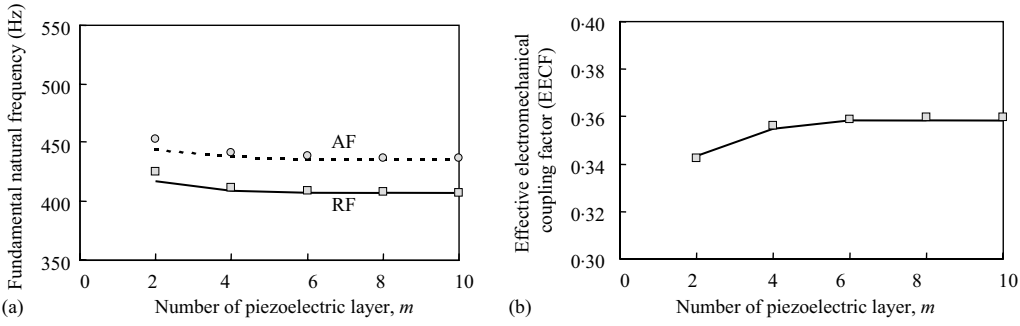

Figure 6. The resonance and antiresonance frequencies (a) and the electromechanical coupling factors (b) of the cantilevered PM in parallel connection versus the number of piezoelectric layers; lines and symbols represent the results by the impedance matrix and the FEM respectively.

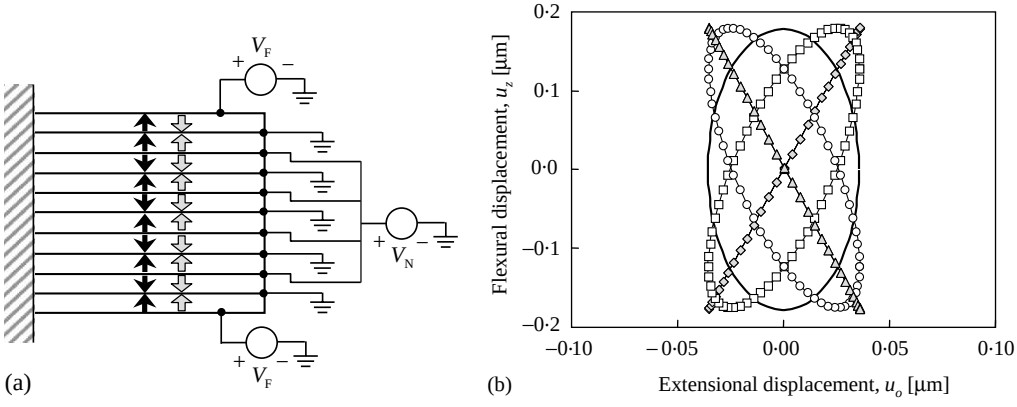

Figure 7. (a) The configuration of the cantilevered multilayer piezomotor ↑, poling direction; ⇧, electric field. (b) $V_N = \cos(\omega t)$ V, $V_F = 2\cos(\omega t + \theta)$ V, $m = 10$; the driving frequency ω is the half of the fundamental RF. The trajectory of the tip under the applied voltage. –◇–, $\theta = 0$; –□–, $\theta = \pi/4$; ——, $\theta = \pi/2$; –●–, $\theta = 3\pi/4$; –▲–, $\theta = \pi$.

flexural RF of the PM. In the numerical calculations, the trajectory of the cantilevered PM tip is calculated by superposing the extensional motion by the voltage V_N and the flexural motion by the voltage V_F. In Figure 7(b), the trajectory of the cantilevered PM tip are shown with respect to the phase difference θ. When θ is $\pi/2$, the trajectory of the PM tip becomes elliptical and its aspect ratio can be changed by the magnitude ratio of V_N and V_F. It is shown that the electromechanical behavior of piezomotor that is in harmonic motion can be easily analyzed using the derived impedance and admittance matrices.

6. CONCLUSION

In this paper, the impedance and admittance matrices of the PM are presented. The extensional and flexural motions have been considered in the derivation. On the assumption of constant electric field in each piezoelectric layer, the motional differential equations for the PM involve only the mechanical material properties and the

electromechanical coupling appears only through the boundary conditions. Using the derived matrices, the static and dynamic characteristics of the cantilevered PM in series or parallel connection are investigated and the tip trajectory of the cantilevered piezomotor is also investigated. The results are compared with those by the FEM and they are in excellent agreement with each other.

It is expected that derived impedance and admittance matrices can be effectively used in analyzing electromechanical systems where external mechanical or electrical components are attached to the PM. The amplitude of the tip deflection or slope near the resonance frequency can be calculated by employing the mechanical, piezoelectric, and dielectric properties in complex variables, which can be determined by experiments. Even in these cases, the expressions for the impedance and admittance matrices will be unaltered. However, since the multimorph considered in this study is thin and narrow, care should be taken in extending the Euler beam theory and the decoupling treatment to a relatively general dimension.

ACKNOWLEDGMENTS

This work was supported by the center of iDOT and the Brain Korea 21 Project.

REFERENCES

1. K. Uchino 1996 *Piezoelectric Actuator and Ultrasonic Motors*. Boston: Kluwer Academic.
2. K. Uchino 1999 *Micromechatronics and Human Science*, 1999. *MHS* '99. Proceedings of 1999 International Symposium on, 3–9. Recent trend of piezoelectric actuator developments.
3. J. G. Smits 1992 *Sensors and Actuators A* 35, 129–135. Design considerations of a piezoelectric on silicon microrobot.
4. C. Lee, T. Itoh and T. Suga 1996 *IEEE Transactions on Ultrasonics, Ferroelectrics, and Frequency Control* **43,** 553–559. Micromachined piezoelectric force sensors based on PZT thin films.
5. Y. Zhao and B. Jones 1997 *Mechatronics* **7,** 11-25. Pulse width modulated reinforced piezo air jet actuators.
6. M. Bexell and S. Johansson 2000 *Sensors and Actuators A* **75,** 118-130. Characteristics of a piezoelectric miniature motor.
7. D. D. Ebenezer 1996 *Journal of the Acoustical Society of America* **99,** 2908–2912. Three-port parameters and equivalent circuit of radially polarized piezoelectric ceramic cylinders of finite length.
8. J. G. Smits and A. Ballato 1994 *Journal of Microelectromechanical Systems* **3,** 105–112. Dynamic admittance matrix of piezoelectric cantilever bimorphs.
9. J. G. Smits, W. Choi and A. Ballato 1997 *IEEE Transactions on Ultrasonics, Ferroelectrics, and Frequency Control* **44,** 250–258. Resonance and antiresonance of symmetric and asymmetric cantilevered piezoelectric flexors.
10. S. K. Ha and Y. H. Kim 2000 *Journal of the Acoustical Society of America* **108,** 2125–2133. Impedance and admittance matrices of symmetric piezoelectric annular bimorphs and their applications.
11. K. Uchino 1998 *Acta Materialia* **46,** 3745–3753. Materials issues in design and performance of piezoelectric actuators: an overview.
12. J. G. Smits, S. I. Dalke and T. K. Cooney 1991 *Sensors and Actuators A* **28,** 41–61. The constituent equations of piezoelectric bimorphs.
13. Q. M. Wang and L. E. Cross 1999 *IEEE Transactions on Ultrasonics, Ferroelectrics, and Frequency Control* **46,** 1343–1351. Constitutive equations of symmetrical triple layer piezoelectric benders.

14. Q. M. Wang, Q. Zhang, B. Xu, R. Liu and L. E. Cross 1999 *Journal of Applied Physics* **86,** 3352–3360. Nonlinear piezoelectric behavior of ceramic bending mode actuators under strong electric fields.
15. Q. M. Wang, X. Du, B. Xu and L. E. Cross 1999 *Journal of Applied Physics* **85,** 1702–1712. Theoretical analysis of the sensor effect of cantilever piezoelectric benders.
16. N. N. Rogacheva, C. C. Chou and S. H. Chang 1998 *IEEE Transactions on Ultrasonics, Ferroelectrics, and Frequency Control* **45,** 285–294. Electromechanical analysis of a symmetric piezoelectric/elastic laminate structure: theory and experiment.
17. S. H. Chang and C. C. Chou 1999 *IEEE Transactions on Ultrasonics, Ferroelectrics, and Frequency Control* **46,** 441–451. Electromechanical analysis of an asymmetric piezoelectric/elastic laminate structure: theory and experiment.
18. Y. S. Cho, Y. E. Park, C. S. Han and S. K. Ha 2000 *Sensors and Actuators A* **84,** 140-148. Five-port equivalent electric circuit of piezoelectric bimorph beam.
19. H. Tanaka 1994 *Journal of the Acoustical Society of America* **95,** 1768–1772. Generalized basic equations for bending motions of piezoelectric bars from Hamilton's principle.
20. R. Aoyagi and H. Tanaka 1995 *Japanese Journal of Applied Physics* **33,** 3010–3014. Equivalent circuit analysis of piezoelectric bending vibrators.
21. *IEEE Standard on Piezoelectricity* 1988 ANSI/IEEE Std. 176–1987, New York: IEEE Inc.
22. Ansys 1995 ANSYS *User's Manual*. Houston, PA: Swanson Analysis Systems, Inc.
23. D. Boucher, M. Lagier and C. Maerfeld 1981 *IEEE Transactions on Sonics and Ultrasonics* **SU-28,** 318–330. Computation of the vibrational modes for piezoelectric array transducer using a mixed finite element-perturbation method.